

Climatic controls on diffuse groundwater recharge in semiarid environments of the southwestern United States

Eric E. Small

Department of Geological Sciences, University of Colorado, Boulder, Colorado, USA

Received 17 March 2004; revised 29 September 2004; accepted 21 January 2005; published 23 April 2005.

[1] Although there is no diffuse groundwater recharge at many semiarid sites, evidence for diffuse recharge exists at some locations where mean annual precipitation \bar{P} is much less than mean annual potential evapotranspiration PET , particularly where soils are coarse and rainfall variable is substantial. We investigate the climatic controls on diffuse recharge using a one-dimensional, variably saturated flow model. The model is driven by a stochastic parameterization of climate that includes storm size distribution and seasonality of precipitation (P) and potential evapotranspiration (PET), constrained by data from 536 weather stations in the southwestern United States. Storm size distribution and seasonality determine the frequency and duration of intervals when P exceeds PET , which controls the flux of water past the root zone. For coarse soils, climates with large, infrequent storms yield recharge when \bar{P}/\overline{PET} exceeds 0.4, compared with 0.7 for a typical climate. Recharge through fine soils is insensitive to storm size and occurs at $\bar{P}/\overline{PET} > 0.8$. Seasonality has a stronger influence on recharge than storm size distribution, and the effects are similar for coarse and fine soils. Recharge is relatively insensitive to rainfall seasonality. In contrast, the typical PET annual cycle lowers \bar{P}/\overline{PET} of the recharge threshold by 0.3. The relative timing of P and PET maxima is critical: Recharge occurs at \bar{P}/\overline{PET} values that are lower by 0.2 when the rainy season occurs during winter instead of summer. Over the range of climate and soils examined, \bar{P}/\overline{PET} values at the recharge threshold varied from 0.2 to 0.7. Therefore \bar{P} and \overline{PET} alone are insufficient to predict where recharge will occur.

Citation: Small, E. E. (2005), Climatic controls on diffuse groundwater recharge in semiarid environments of the southwestern United States, *Water Resour. Res.*, 41, W04012, doi:10.1029/2004WR003193.

1. Introduction

1.1. Diffuse Recharge

[2] Groundwater recharge is considered to occur via two pathways in arid and semiarid regions. First, focused recharge occurs at locations where surface water flow is concentrated, including streams channels [Sorman *et al.*, 1997; Izbicki *et al.*, 2000; Houston, 2002], playas or topographic depressions [Allison *et al.*, 1985; Wood and Sanford, 1995], fissures or pipes [Scanlon, 1992; Johnston, 1987], and irrigated areas [Leaney and Herczeg, 1995]. Although focused recharge only occurs in a fraction of the landscape, it may be the primary mechanism recharging aquifers in many basins, as the recharge rates are high. Second, precipitation may infiltrate where it hits the ground and move vertically to the water table, yielding diffuse recharge [Hendrickx and Walker, 1997; Phillips, 1994]. Diffuse recharge is expected to be much slower than focused recharge. However, it may be a significant component of a basin's water balance if rates are nonzero over extensive areas [Hendrickx and Walker, 1997]. Identifying where and when diffuse recharge occurs is necessary for water resource management and assessing the risk of

hazardous waste storage in the vadose zone [Mann, 1976; Nativ, 1991].

[3] Previous studies have shown that there is currently no diffuse recharge at many arid and semiarid sites worldwide [Phillips, 1994; Scanlon *et al.*, 1999; Izbicki *et al.*, 2000], where the mean annual precipitation rate (\bar{P}) is much less than mean annual potential evapotranspiration rate (\overline{PET}). At these sites, the distribution of environmental tracers indicates there is little downward movement of water below the root zone, on timescales of decades to millennia (reviewed by Phillips [1994]). This is consistent with measured vertical profiles of water potential [Izbicki *et al.*, 2000]. Lysimeter studies also show that deep percolation does not occur under natural vegetation conditions [Gee *et al.*, 1994].

[4] Although there is no diffuse recharge at many sites, previous studies reported evidence for diffuse recharge at some locations where $\bar{P}/\overline{PET} \ll 1$ (reviewed by Stephens [1994]). At these sites, evidence for diffuse recharge was derived from similar types of data as used in studies that have found no recharge, including environmental tracers [Edmunds *et al.*, 1988], well hydrographs [Barnes *et al.*, 1994], lysimeters [Gee *et al.*, 1994], and measurements of vertical gradients in hydraulic head [Stephens and Knowlton, 1986; Grismer *et al.*, 2000]. Many studies that found evidence of no diffuse recharge were carried out in the driest and hottest locations [e.g., Tyler *et al.*, 1996]. At

higher elevations or in wetter climates, $\overline{P/PET}$ may be high enough so that diffuse recharge occurs. In addition, at many sites where there is currently no diffuse recharge, the inventory of meteoric chloride in soil shows that diffuse recharge did occur $\sim 10\text{--}15$ kya [Phillips, 1994] or during even earlier glacial periods [Tyler *et al.*, 1996; Scanlon *et al.*, 2003]. Simulations of coupled liquid and vapor flow and the associated transport of chloride are consistent with this interpretation [Walvoord *et al.*, 2002a, 2002b; Scanlon *et al.*, 2003].

1.2. Factors Controlling Diffuse Recharge

[5] Previous research shows that diffuse recharge occurs in some semiarid locations but not others, and at some times but not others. Therefore there are two critical questions regarding diffuse recharge in semiarid environments: (1) What factors and processes control whether or not diffuse recharge occurs at a particular location? (2) What controls the fraction of precipitation that recharges groundwater where recharge does occur?

1.2.1. Observations

[6] On the basis of data collected from semiarid environments, the following factors have been suggested as controlling where and when diffuse recharge occurs. First, diffuse recharge is expected to be greater through coarse soils than fine soils, because wetting fronts propagate more deeply into coarse soils. The soil was relatively coarse (sand or loamy sand) at most of the sites where evidence for recharge was found in a climate where $\overline{P/PET}$ is $\ll 1$ [Stephens, 1994; Barnes *et al.*, 1994]. Second, the presence and type of vegetation are believed to play a key role in controlling diffuse recharge [Mann, 1976; Fayer *et al.*, 1996; Allison *et al.*, 1990; Phillips, 1994]. At sites in New Mexico and Nevada, Gee *et al.* [1994] found that water accumulated in deep lysimeters that were kept vegetation free, whereas deep percolation did not occur in lysimeters at the same sites with growing vegetation. Desert vegetation, such as the shrub *Larrea* (Creosotebush), have relatively deep root systems [Schenk and Jackson, 2002] and transpire until soil water potential is highly negative (-8 MPa) [Pockman and Sperry, 2000]. Because desert plants are able to remove nearly all water from the top several meters of soil, it has been hypothesized that the transition to desert plant species at the end of the Pleistocene (~ 10 kyr) is the cause of the shift to the no-diffuse recharge regime observed at many sites [Phillips, 1994; Walvoord *et al.*, 2002b]. Third, variability of hydrometeorological conditions is believed to strongly control whether or not diffuse recharge occurs: The precipitation rate (P) may exceed the potential evapotranspiration rate (PET) over some interval, even though $\overline{P/PET} < 1$. The occurrence of a single large precipitation event or a series of events may yield diffuse recharge [Barnes *et al.*, 1994; Stephens, 1994]. A climate with primarily winter precipitation may also yield diffuse recharge. PET is relatively low during these months so water can penetrate more deeply into the soil than during the summer months, as indicated by soil water potential measurements [Gee *et al.*, 1994; Andraski, 1997; Grismer *et al.*, 2000]. The importance of cold season precipitation may be enhanced in environments where vegetation is dormant in the winter due to temperature limitations [e.g., Scott *et al.*, 2000]. Variability on interannual timescales is also

important: Recharge may only occur during particularly wet years.

1.2.2. Modeling

[7] In many previous studies, models have been used to study how precipitation is partitioned into runoff, evapotranspiration (ET), and percolation in semiarid environments [Scott *et al.*, 2000; Laio *et al.*, 2001]. In fewer cases, models have been used specifically to provide constraints on recharge in semiarid environment. The model structures used in both types of studies are variable. In the vertical direction, both one- or two-layer bucket models [Beverly *et al.*, 1999; Laio *et al.*, 2001; Hevesi *et al.*, 2002] and models with fine vertical discretization [Rockhold *et al.*, 1995; Kearns and Hendrickx, 1998] have been used. In the horizontal direction, models represent either a single point [Scott *et al.*, 2000] or multiple points across a landscape that may differ with regards to elevation, soil thickness, or other properties [Fayer *et al.*, 1996]. The loss of water via evapotranspiration (ET) has been represented in various ways, including lumped ET loss terms [Laio *et al.*, 2001], root water uptake controlled by soil moisture stress and root density functions [Kearns and Hendrickx, 1998], and as a head boundary condition [Walvoord *et al.*, 2002a].

[8] The few modeling studies focused on diffuse recharge support the inferences made from observations. First, simulated recharge or deep percolation is greater through coarse soils than fine soils [Kearns and Hendrickx, 1998; Rockhold *et al.*, 1995; Fayer *et al.*, 1996]. Second, vegetation limits or precludes diffuse recharge [Kearns and Hendrickx, 1998], and xeric shrubs limit recharge the most [Fayer *et al.*, 1996]. For simple bucket models, the bottom flux is greater for shallower root zones [Laio *et al.*, 2001] or for shallower soils [Hevesi *et al.*, 2002]. Third, temporal fluctuations in P and PET are critical where $\overline{P/PET} < 1$. Using a 100-year-long rainfall record from New Mexico, Kearns and Hendrickx [1998] found that deep percolation only occurred during five intervals with particularly high rainfall. Also using observed rainfall records, several studies show that simulated recharge or deep percolation occurs primarily during winter and is greatest during wet winters [Rockhold *et al.*, 1995; Fayer *et al.*, 1996; Scott *et al.*, 2000].

1.3. Goals of This Study

[9] Here we use a one-dimensional vadose zone model to evaluate how climate controls diffuse recharge, focusing on how the temporal variability of P and PET controls whether or not diffuse recharge occurs in locations where $\overline{P/PET} < 1$. We test the following two hypotheses. First, a climate characterized by relatively large storms should be favorable for diffuse recharge. Second, climates with relatively high fractions of precipitation falling during the winter months should yield more diffuse recharge. Previous modeling studies of recharge in semiarid environments used P and PET observed at single locations [Rockhold *et al.*, 1995; Fayer *et al.*, 1996; Kearns and Hendrickx, 1998; Hevesi *et al.*, 2002]. Therefore these studies were not designed to assess how variations in climate through space control recharge. In contrast, we describe climate using a limited number of parameters. Then, we generate meteorological inputs for our flow simulations using these parameters and assess how these climatic factors influence diffuse recharge. Our model of climate represents (1) seasonal variations in P

Table 1. Soil Hydraulic Properties for the *van Genuchten* [1980] Model From the Rosetta Database [Schaap *et al.*, 1998] for Loamy Sand and Loam Soils Used in Simulations^a

	θ_r	θ_s	α	n	K_{s_s} , cm d ⁻¹	λ
Loamy sand	0.049	0.39	0.035	1.75	105	-0.874
Loam	0.061	0.399	0.011	1.47	12.1	-0.371

^a θ_r and θ_s are residual and saturated water content, respectively (cm³ cm⁻³); α (cm⁻¹), n , and λ are curve shape parameters; K_{s_s} is conductivity at saturation.

and *PET* and (2) the distribution of storm sizes. We compare the role of climate for both coarse and fine soils.

[10] Our goal is not to predict the magnitude of diffuse recharge for a particular set of climate conditions. Instead, we explore and identify the most important climatic factors and their interactions. To focus on the various aspects of climate, it is necessary to generalize and simplify other processes. We do not address several important aspects of water flow in semiarid vadose zones, including variability of soil texture, preferential flow through macropores, and surface water redistribution. We characterize vegetation as typical plants found in desert environments. In the next section we describe the flow model used in this study. Then we introduce the model of climate used to generate the meteorological inputs for our simulations. This is followed by a description of results and a discussion.

2. Flow Model

2.1. Variably Saturated Flow

[11] We model one-dimensional vertical flow of liquid water by solving the hydraulic head form of the Richards equation for variably saturated flow

$$C(h) \frac{\partial h}{\partial t} = \frac{[K(h) \left(\frac{\partial h}{\partial z} + 1 \right)]}{\partial z} - S(h), \quad (1)$$

where $C(h) = d\theta/dh$ is the specific water capacity function (cm⁻¹), h is the hydraulic head (cm), $K(h)$ is the hydraulic conductivity (cm s⁻¹), z is the vertical coordinate, and S is the root extraction term (cm³ cm⁻³ s⁻¹). Our solution of equation (1) is the same as that used in the SWAP model [van Dam *et al.*, 1997; van Dam and Feddes, 2000]. The model employs a finite difference, fully implicit solution to equation (1). $K(h)$ is calculated arithmetically for the component of flow driven by the matric potential gradient [Simunek *et al.*, 1998; van Dam and Feddes, 2000]. $K(h)$ from the higher of two layers is used for the component of flow driven by gravity. For each time step, the changes in h are determined iteratively. The convergence criteria is 10⁻⁴ in θ when the soil is unsaturated, and 0.01 cm in h when the soil is saturated [Huang *et al.*, 1996; van Dam and Feddes, 2000]. The time step is adjusted within the range of 0.025 to 8640 s, depending upon the number of iterations required for convergence. Mass balance is calculated at each node following each time step, and its error never exceeds 10⁻³ in the simulations described below.

[12] We use 57 depth increments between the surface and 10 m. Layer thickness is 1 cm at the top and increases by a factor of 1.08 for each depth increment, yielding thicknesses of 0.35 m and 0.75 m at the middle and bottom of the

domain, respectively. This arrangement (1) allows for a detailed representation of the large gradients near the surface, (2) allows for storage beneath the root zone, and (3) minimizes computational time. Including the thick soil zone below the deepest roots is necessary because water uptake by plants yields upward flow into the root zone during dry periods. The domain used here is not the same as a soil thickness of 10 m in bucket-model simulations [e.g., Laio *et al.*, 2001; Hevesi *et al.*, 2002]. In these simulations the simulated recharge or drainage varies with bucket depth and therefore storage capacity. In a series of test simulations we found that simulated recharge did not depend on domain length if the thickness below the root zone exceeded several meters. Simulations using the layer dimensions described above were compared with test simulations with constant layer thickness of 1 cm, and only negligible differences were found.

[13] All simulations were completed for two different soil types: loamy sand and loam. Water retention and unsaturated hydraulic conductivity curves were specified according to the *van Genuchten* [1980] model, with soil hydraulic parameters specified according to the Rosetta database [Schaap *et al.*, 1998] (Table 1). We did not choose sand for the coarser of the two soil types because this would have made it difficult to generalize our results for less extreme textured soils such as sandy loams.

2.2. Boundary Conditions

[14] The flux at the bottom boundary of the model, q_b , was set to gravity drainage, scaled by $K(h)$ of the bottom layer. As described in more detail in section 2.3, we assume that q_b is diffuse groundwater recharge, even though the water table is not explicitly modeled. This assumption is based on the idea that if water moves >7 m below the deepest roots, it will eventually reach the groundwater table. The top surface boundary condition depends on the throughfall and *PET* rates, as described by van Dam and Feddes [2000]. The model includes an interception reservoir with a depth of 0.1 cm, and precipitation only yields throughfall when the interception reservoir is full. We calculate the maximum possible flux through the surface node, q_t^{\max} , based on the gradient in h and $K(h)$. When there is throughfall, the flux through the surface boundary, q_t , is set to the throughfall rate if q_t^{\max} is greater than or equal to the throughfall rate. Otherwise, $q_t = q_t^{\max}$ and h at the surface (h_{top}) is set to 0 cm. In this case, throughfall in excess of q_t is considered runoff as we assume no ponding.

2.2.1. Evaporation From Soil

[15] When it is not raining, the direct evaporation flux E is calculated according to several constraints, as was done by van Dam and Feddes [2000]. First, if there is water in the interception reservoir, then direct evaporation from plant surfaces proceeds at the *PET* rate, and the flux at the soil surface and transpiration are zero. Second, if there is no interception loss, E is calculated by specifying either the head or flux at the surface. If q_t^{\max} exceeds the *PET* rate, then E equals *PET*. Otherwise h_{top} is prescribed to that of the atmosphere, h_{atm} , and E is set to q_t^{\max} . Specifying h_{atm} to the extremely low values that exist at the soil-atmosphere interface (~ -50 MPa) is unnecessary because liquid flow is effectively zero at the associated water contents. However, it is important that h_{atm} is less than the wilting point of the

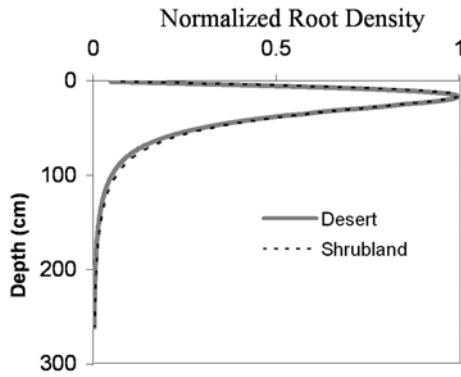


Figure 1. Vertical variations in root density, normalized to a value of 1, for both desert vegetation and semiarid shrubland from the *Schenk and Jackson* [2002] data set. The desert profile is used here. Maximum root depth is 2.6 m. The total thickness of the model domain is 10 m.

vegetation (h_{wilt}), so that direct evaporation may proceed even after transpiration has stopped [Laio *et al.*, 2001]. Therefore we set h_{atm} to -15 MPa, which is significantly lower than the wilting point used. In a series of test simulations, we found that varying h_{atm} between -7 and -20 MPa did not affect the simulated recharge.

2.2.2. Transpiration

[16] Simulating root water uptake from a soil with vertical variations in h and root density is challenging and poorly constrained [Sperry, 2000; Guswa *et al.*, 2002; Lai and Katul, 2000]. Therefore we use a relatively simple approach that is included in a broad range of models [Mahfouf *et al.*, 1996; Simunek *et al.*, 1998; Feddes *et al.*, 2001]. At each model level, i , root water uptake is restricted according to a soil-water availability factor γ_i that depends on h

$$\begin{aligned} \gamma_i &= 0.0, h_i \leq h_{wilt} \\ \gamma_i &= \frac{h_i - h_{wilt}}{h^* - h_{wilt}}, h_{wilt} < h_i < h^* \\ \gamma_i &= 1.0, h_i \geq h^* \end{aligned} \quad (2)$$

Below h_{wilt} , γ_i equals zero and there is no root water uptake from that layer. Between h_{wilt} and the head value at which uptake is not limited by soil water h^* , γ_i increases linearly with h_i . Above h^* , γ_i equals one and root water uptake is not limited by soil water availability. We use values of -5 MPa and -0.1 MPa for h_{wilt} and h^* , respectively, consistent with measurements from desert vegetation [Pockman and Sperry, 2000].

[17] The root water uptake at any model layer, S_i , is

$$S_i = \beta \gamma_i r_i dz_i \quad \text{for } z_i \leq z_r, \quad (3)$$

where r_i is the fraction of all roots in that model layer (unitless), dz_i is the layer thickness (cm), β is a scaling factor described below ($\text{cm}^2 \text{cm}^{-3} \text{s}^{-1}$), and z_r is the total depth of the root zone. The vertical distribution of roots with depth, $r(z)$, is prescribed according to the model of *Schenk and Jackson* [2002], using parameters for “desert” vegetation

(Figure 1), which are nearly identical to the parameters for “semiarid shrubland.” The depth above which 95% of the roots are found, d_{95} , is 1.3 m for desert vegetation. In the *Schenk and Jackson* [2002] model, r decreases with depth but never reaches zero. We specify z_r as equal to $2 \times d_{95}$, which encompasses 99% of the roots in the distribution. We specify z_r because it is uncommon to find roots to a depth of 10 m in nonriparian environments [Canadell *et al.*, 1996]. In test simulations we found that specifying z_r rather than including roots throughout the domain does not influence the calculated recharge rate.

[18] The total transpiration T is the sum of root water uptake at each layer with roots

$$T = \sum_{i=\max}^{i=1} S_i. \quad (4)$$

The scaling factor β in equation (3) is calculated so that transpiration only equals PET when γ_i is 1.0 everywhere. This formulation is based on the assumption that plants cannot compensate for part of their roots being in dry soil [Guswa *et al.*, 2002]. If the sum of T and E exceeds PET , then both are reduced so that ET equals PET and the ratio of T and E is preserved. In this case, the root water uptake from each level is scaled accordingly.

2.3. Initialization and Simulation Length

[19] At the start of each simulation, h at all model layers is set to the wilting point, h_{wilt} . Initialization to drier values has little impact, because only a small amount of water is needed to wet soil to h_{wilt} . Initialization to wetter values makes it difficult to calculate recharge in cases with little or no diffuse recharge: Meaningful estimates can only be made once the entire soil column drains from the initially wet value. Initially, there is a very slow flux due to gravity drainage from the bottom of the model domain, q_b , which is ~ 7 orders of magnitude slower than the prescribed rainfall rates. In many simulations, wetting fronts never propagate below the root zone and q_b slowly decreases. Clearly, this flux should not be considered as recharge because it simply reflects the choice of initial conditions. Therefore we only begin calculating recharge once

$$q_b \geq 0.0001 \times \bar{P} \quad (5)$$

for the first time during a simulation. For example, if \bar{P} is 50 cm yr^{-1} , then recharge is only calculated after q_b exceeds 0.05 cm yr^{-1} for the first time. This recharge threshold was chosen to reflect the limit of where our liquid-only flow model is applicable. When $q_b < 0.0001 \times \bar{P}$, the liquid flux is often similar to or slower than the upward vapor flux driven by thermal gradients [Ross, 1984; Walvoord *et al.*, 2002a], and the liquid-only flow model may not be applicable.

[20] Given stochastic rainfall inputs and the nonlinear processes operating in the vadose zone, it is not possible to assess a priori how long simulations need to be so that the calculated recharge rate is representative of the prescribed soil and climate parameters. Therefore we completed a series of test simulations to assess how the simulated recharge rate varied through time. When the portion of rainfall that is partitioned to recharge, $\%R$ (reported as a percentage of \bar{P}), is less than 1%, a representative recharge

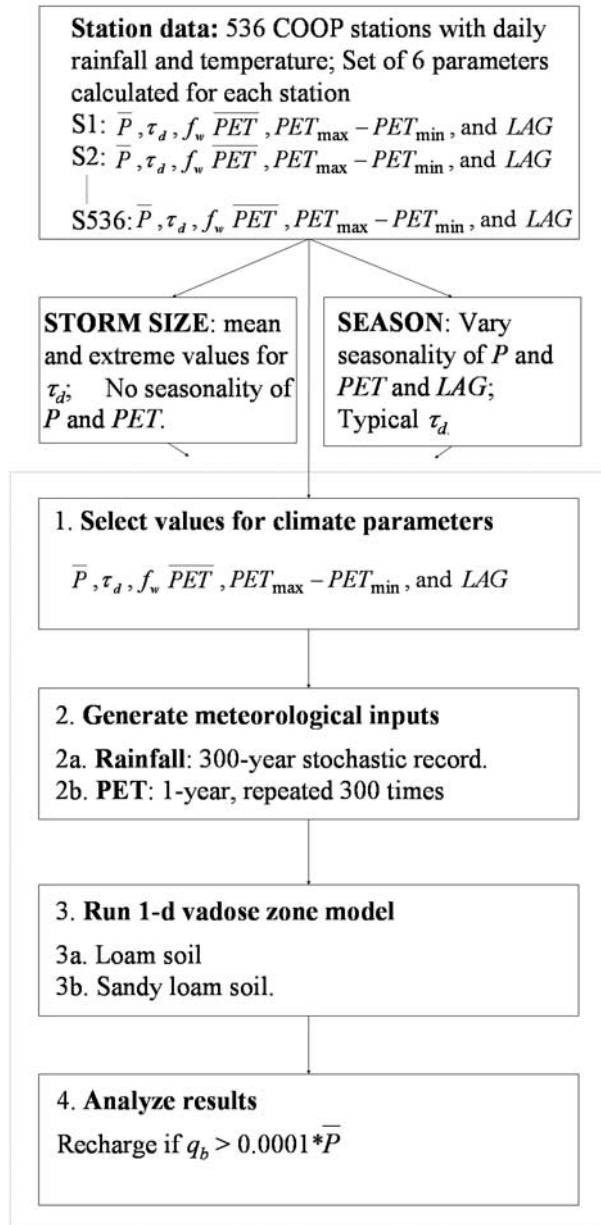


Figure 2. Steps taken to use station data to generate meteorological inputs for the flow model. Daily rainfall and temperature time series are analyzed to calculate the six parameters of the climate model (top box). The parameter set from each station can be used directly to generate P and PET records. Alternatively, parameter values can be varied across the range that exists within the station data (storm size or season experiments) and then used to generate P and PET records. The bottom four panels show the four steps taken to complete each individual simulation.

rate is only attained when the simulation length exceeds 100 years. Therefore all simulations were run for 300 years, with the first 30 years excluded from calculations to minimize the influence of initial conditions. Given that long simulations were necessary, we did not use observed precipitation records, which are often only 30–40 years long.

Instead, we generated 300-year-long stochastic rainfall records [e.g., *Eagleson, 1978*] constrained by observations from weather stations.

3. Climate Model and Simulations

[21] In this section, we describe (1) how we use station data to estimate the parameters of a climate model that characterizes P and PET ; (2) how we stochastically generate P and PET records based on these parameters; and (3) the various model simulations completed. This approach is summarized in Figure 2. Our model of climate was developed to satisfy three considerations. First, the model must represent the climatic features hypothesized to influence recharge in previous research. Second, the model must have as few parameters as possible, so that the influence of each parameter can be quantified. Third, observations must exist to constrain the range of each model parameter. On the basis of past research, we included six parameters in our model. For rainfall, the climate is characterized by the mean annual precipitation rate, storm size distribution, and a seasonality index. For PET , the mean annual value and seasonal amplitude are specified. The timing of seasonal cycles of P and PET are related via a lag value.

3.1. Rainfall

3.1.1. Stochastic Model of Rainfall Events and Seasonality of Rainfall

[22] We model rainfall as a Poisson process on the daily timescale [*Eagleson, 1978; Rodriguez-Iturbe et al., 1999*]. The distribution of dry intervals length (τ , in days) between rainfall events is exponential

$$f_T(\tau) = \frac{1}{\tau_d} e^{-\frac{\tau}{\tau_d}}, \quad (6)$$

where τ_d is the mean dry interval time, in days. The distribution of storm depth is also exponential, with a mean depth of α (cm). Because the soil moisture model operates on time steps much shorter than days, we must also specify a rainfall rate for each event, again modeled as an exponential distribution [*Guswa et al., 2002*]. There is no correlation between τ_d , α , and rainfall rate. The relationship between the mean annual precipitation rate \bar{P} and the values for τ_d and α is

$$\bar{P} = \alpha / \tau_d. \quad (7)$$

So if \bar{P} and either τ_d or α is prescribed, the remaining parameter can be calculated.

[23] Seasonal variations in rainfall are not represented by the simple Poisson model [*Rodriguez-Iturbe et al., 1999*], but seasonality may strongly influence recharge. Seasonal rainfall variations can be represented within the Poisson model framework by specifying τ_d and α for each month separately [*Hawk and Eagleson, 1992*], requiring a large number of parameter values. To minimize the number of parameters values needed, we split each year into a wet and dry season, each receiving half of the mean annual precipitation (Figure 3). The wet season was identified as the shortest continuous period of the year during which 50% of the annual rainfall accumulates. The wet season duration is a fraction of the year, f_w , with a maximum value of 0.5 in the

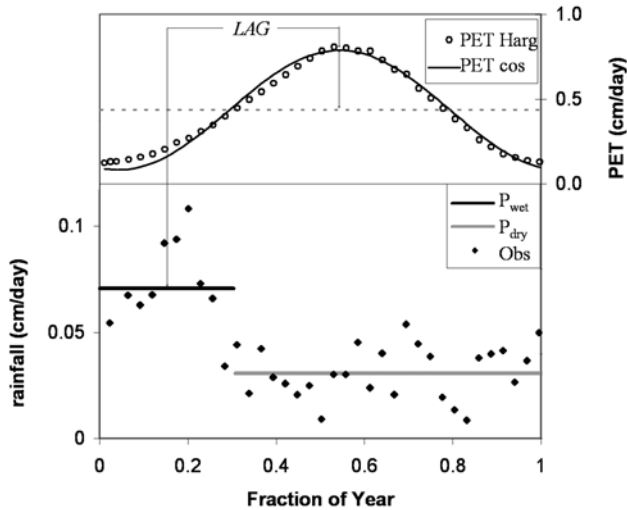


Figure 3. Sketch of the climate parameterization used here. The parameters and data shown in this figure are derived from the Beatty, Nevada, COOP station. The x -axis shows fraction of year, with 0.0 set to the beginning of the wet season. In the top portion of the panel, open circles show seasonal fluctuations of PET calculated using the Hargreave’s equation (equation (11)) and daily station data. The solid line shows PET calculated according to the sinusoidal PET model (equation (12)), parameterized using the Hargreave’s \overline{PET} and $PET_{\max} - PET_{\min}$ values. The dashed line shows \overline{PET} , and the thin vertical line between the solid and dashed curves is equal to $0.5 \times PET_{\max} - PET_{\min}$. In the bottom portion, data points show observed rainfall from the 40-year rainfall record, averaged over 10-day intervals. The wet season duration is 0.31, and the solid lines show the average rainfall values used in the wet and dry seasons. The lag between the middle of the wet season and the PET maximum, LAG , is shown.

case of no seasonality. The dry season is the remainder of the year, with fractional duration $(1 - f_w)$. The duration of each season, the rainfall rate in that season (subscripts wet or dry), and the mean annual rainfall rate \overline{P} are related as follows:

$$P_{wet} = \frac{0.5\overline{P}}{f_w}, \quad P_{dry} = \frac{0.5\overline{P}}{(1 - f_w)}. \quad (8)$$

3.1.2. Constraints From Rainfall Data

[24] We used daily rainfall and temperature data from more than 700 weather stations, all part of the National Weather Service’s Cooperative Observer Program (COOP), in the southwestern United States to constrain parameters of our climate model. All records from currently operating stations in Arizona, Nevada, New Mexico, Utah, and Texas west of -101 longitude were used. In addition, 65 stations with $\overline{P} < 100 \text{ cm yr}^{-1}$ were selected from California. Only records that exceeded 35 years in duration were used in the following analyses, for a total of 536 station records and more than 1.25×10^7 days of data. The wide geographic distribution of the stations ensures that we have sampled across a broad range of semiarid climates types.

3.1.2.1. Annual Timescale

[25] A wide range of combinations of τ_d and α can yield the same value of \overline{P} (Figure 4a). For example, at some stations where $\overline{P} = 35 \text{ cm/year}$, α is $\sim 1 \text{ cm}$ and τ_d is ~ 10 days; large storms occur infrequently. At other stations, α is $< 0.5 \text{ cm}$ and τ_d is as short as 4 days, showing that rainfall occurs frequently but storm sizes are small. The

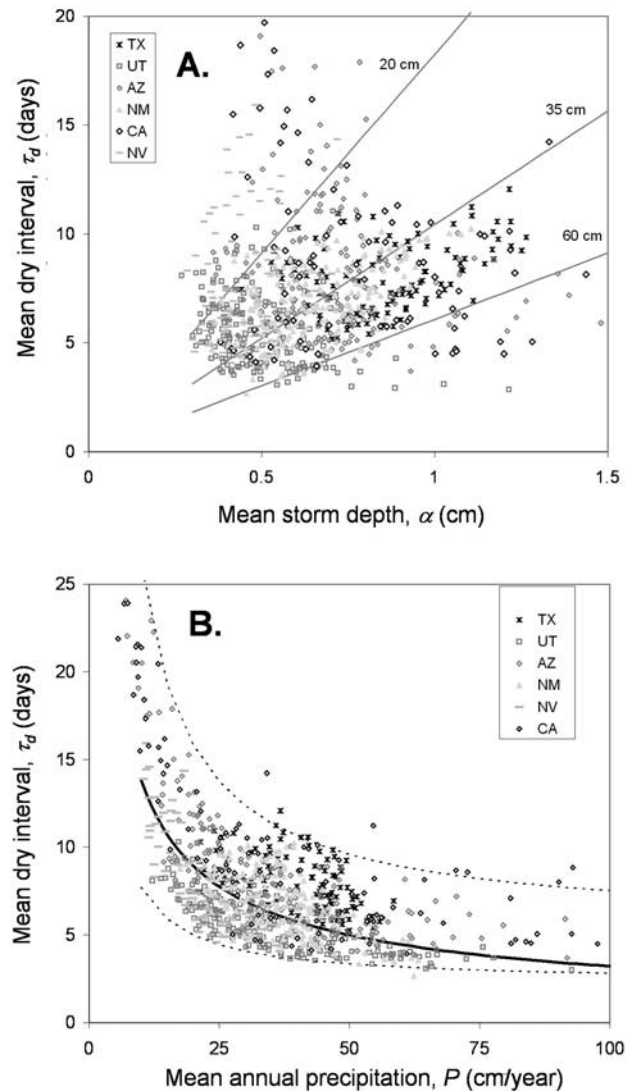


Figure 4. (a) Mean dry interval (τ_d) versus mean storm depth (α) for southwestern U.S. stations. The various symbols represent the different states. Lines of equal \overline{P} are drawn and labeled. (b) Relationship between τ_d and \overline{P} . The solid line is the best fit power law curve to all data points ($r^2 = 0.51$), used in the “typical storm size” simulations (Table 4). Dashed lines are envelopes using the same equation form, with parameters selected so that the lines encompass all but the extreme outliers. The top dashed curve represents the $\tau_d - \overline{P}$ relationship where dry intervals are long and storms are large, used in the “maximum storm size” simulations. The bottom line represents the $\tau_d - \overline{P}$ relationship where storms are frequent but small, used in the “minimum storm size” simulations. See color version of this figure at back of this issue.

Table 2. Wet Season Duration (f_w) and the Middle of the Wet Season, Reported as Day of Year, From the Southwestern U.S. COOP Station Data

State	f_w	Middle of Wet Season
All	0.32	
Arizona	0.33	184
California	0.25	31
New Mexico	0.27	225
Nevada	0.38	80
Texas	0.29	205
Utah	0.40	139

variability in storm size distribution is geographically coherent. For the same \bar{P} , τ_d and α tend to be greater in Texas, Arizona, and California than in Utah and Nevada. A power law relationship between mean annual precipitation and mean dry interval was developed using a least squares fit ($r^2 = 0.51$) to the composite data set of τ_d and \bar{P} (Figure 4b):

$$\tau_d = 53.7\bar{P}^{-0.59}. \quad (9)$$

In our model experiments (section 3.3), we use this relationship to estimate typical values of τ_d given some \bar{P} . Then we calculate α according to equation (7). We did not use the reverse procedure because the relationship between α and \bar{P} is very weak.

3.1.2.2. Seasonality

[26] The station data also provide constraints on the seasonality of precipitation and how the seasonality reflects combined changes in τ_d and α . On average, the wet season is 32% of the entire year ($f_w = 0.32$) or 4 months long (Table 2), so the rainfall rate is 2.3 times higher in the wet season than in the dry season. There is substantial variability in the duration of the wet season, both between states (Table 2) and from station to station.

[27] The higher rainfall rate during the wet season is primarily the result of a reduction in τ_d compared with the annual average, equivalent to an increase in storm frequency ($1/\tau$). The increase in storm frequency is accompanied by relatively small increases in storm size (α). Similarly, the lower rainfall rate during the dry season is due primarily to an increase in τ_d or a decrease in storm frequency. We compare the seasonal changes in storm size and frequency to seasonal changes in rainfall rate in Figure 5, for both the wet and dry season. We plot seasonal values of precipitation α and $1/\tau_d$ normalized by the annual average values, for each station in the data set. During the wet season, the normalized increase in storm frequency is roughly 70% as large as the normalized increase in rainfall rate, so the points for storm frequency fall close to the 1:1 line in Figure 5. In contrast, the normalized increase in storm size is only $\sim 10\%$ as large, so storm size points fall along a line with much lower (or zero) slope. The changes in the dry season are similar: Storm frequency decreases greatly whereas storm size remains nearly the same. We use the best fit relationship in Figure 5 ($r^2 = 0.89$),

$$\tau_{d,season}/\tau_d = 0.70(P_{season}/\bar{P}) + 0.30, \quad (10)$$

to predict the wet and dry season values of dry interval length ($\tau_{d,season}$) from seasonal rainfall rate (P_{season}) and the

annual values of τ_d and \bar{P} . Seasonal variations in storm size are then calculated according to equation (7).

[28] Throughout the southwestern United States, the middle of the wet season falls within four distinct different periods (Table 2): (1) during winter in California, western Arizona, southwestern Utah, and southern Nevada; (2) during early spring in the great basin of Nevada and Utah; (3) during late spring in eastern New Mexico and northwestern Texas; and (4) during midsummer in western New Mexico, eastern Arizona, and Utah, and western Texas south of 32°N . In our model, the timing of the wet season is only important when considered relative to the seasonal fluctuations of PET , which we discuss in the next section.

3.2. Potential Evapotranspiration and Seasonal Fluctuations of PET

[29] The PET boundary condition sets the maximum rate of water loss from the top boundary of the model domain. As we show below, our conclusions do not depend upon the magnitude of our PET estimates: Results are presented in terms of \bar{P}/PET and the sensitivity to the actual values of PET used is minimal. This is important considering methods to estimate PET were developed for crops [Shuttleworth, 1993], not for the semiarid environments modeled here. As bounds for the model experiments, we seek constraints on how PET varies across the southwestern United States, in particular how PET varies throughout the year.

[30] A variety of methods have been established to estimate PET from meteorological data [Shuttleworth, 1993]. The Penman-Monteith (PM) equation is believed to provide the best estimate of reference crop PET , but the data requirements for PM are substantial and are typically only satisfied with reliable data at heavily instrumented research sites [Shuttleworth, 1993; Allen et al., 1998; Droogers and Allen, 2002]. Maximum and minimum temperatures are the only meteorological variables measured at the COOP sta-

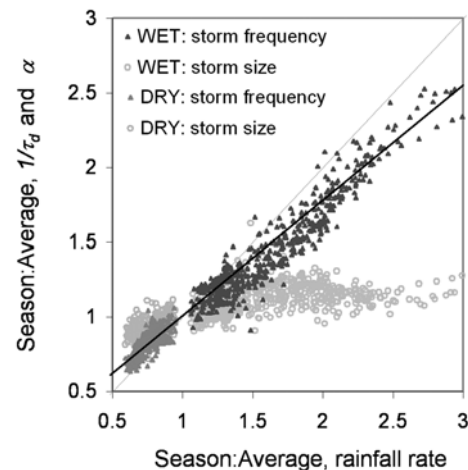


Figure 5. Scatterplot of the ratios of season-to-average $1/\tau_d$ (triangles) and α (circles) versus the ratio of season-to-average rainfall rates for all COOP stations. The ratios for both the wet (light and dark blue points) and dry (orange and red symbols) seasons are shown. The thin line is the 1:1 line, and the thick line is the best fit linear regression to the normalized wet and dry season $1/\tau_d$ values (equation (10)). See color version of this figure at back of this issue.

Table 3. PET Statistics Derived From Southwestern U.S. COOP Station Temperature Data and Calculations of S_0

Region	PET, mm d ⁻¹		L_{PET} , days	
	\overline{PET}	$PET_{\max} - PET_{\min}$	Summer	Winter
All	4.09	6.37	11.3	10.8
Arizona	4.09	6.27	21.0	6.8
California	4.51	6.63	5.4	10.9
New Mexico	4.03	6.24	5.5	12.0
Nevada	3.66	6.71	21.2	9.2
Texas	4.41	5.80	6.2	13.7
Utah	3.48	6.67	16.6	12.1

tions that can be used to estimate PET . Therefore we use the Hargreaves equation [Hargreaves and Samani, 1982] to estimate PET (mm d⁻¹) from temperature data in conjunction with calculations of solar radiation:

$$PET = aS_0(T_{avg} + b)(T_{\max} - T_{\min})^{0.5}. \quad (11)$$

T_{avg} is the average temperature (°C) calculated from daily maximum and minimum temperatures, T_{\max} and T_{\min} , and S_0 is the evaporated water-depth equivalent of solar radiation (mm day⁻¹) at the top of the atmosphere. The Hargreaves equation is empirically based, but the first term (S_0) provides an energy constraint, the second ($T_{avg} + b$) varies nearly linearly with the thermodynamic scaling term in the Penman combination equation, and the third ($(T_{\max} - T_{\min})^{0.5}$) indirectly factors in cloudiness [Shuttleworth, 1993]. We use the parameter values ($a = 0.0025$ and $b = 16.8$) from Droogers and Allen [2002], who calibrated the Hargreaves parameters via a comparison with PM estimates derived from a coarse-resolution, global meteorological data set. These globally derived parameter values yield \overline{PET} that is similar to PM reference crop \overline{PET} in the southwestern United States, although values tend to be too low by ~ 1 mm d⁻¹ in Texas and Arizona south of roughly 33°N [Droogers and Allen, 2002, Figure 2].

[31] The annual cycle of PET calculated using the Hargreave's equation (equation (11)) and daily station data is sinusoidal (Figure 3). Therefore we developed the following model for seasonal fluctuations in PET :

$$PET(DOY) = \left(\frac{PET_{\max} - PET_{\min}}{2} \right) \cdot \cos \left[2\pi \left(\frac{DOY - L_{PET} - 365/2}{365} \right) \right] + \overline{PET} \quad (12)$$

where DOY is calendar day of year, PET_{\max} and PET_{\min} are the maximum and minimum values throughout the year, \overline{PET} is the mean annual PET rate, and L_{PET} is the lag of peak ET behind peak solar forcing (in days). We calculate the annual cycle of PET using the Hargreaves equation. Daily solar radiation is determined from the latitude of the site. T_{avg} and $T_{\max} - T_{\min}$ are set to the average values for each DOY. Only data from stations with records that exceeded 35 years were used. The PET_{\max} and PET_{\min} values are determined from the 9-day periods within the annual cycle that have the highest and lowest values. L_{PET} is calculated using the midpoint DOY of the 9-day interval with the highest PET compared with the day with peak S_0 . For each station, PET estimated via the sinusoidal model (equation (12)) is very similar to the seasonal cycle of PET calculated using the Hargreave's equation (equation (11)) and daily station data (e.g., Figure 3), although the latter tends to have a broader bottom and a higher, narrower peak.

[32] Averaged over all stations, \overline{PET} is 4.1 ± 0.7 mm d⁻¹ or roughly 150 cm year⁻¹ (Table 3). The variability between stations is limited compared with that of the rainfall parameters. At individual stations, \overline{PET} values vary from 3.5 mm d⁻¹ to 6.5 mm d⁻¹. Much of this variability is related to station elevation: \overline{PET} decreases linearly by ~ 1 mm d⁻¹ per 1000 m of station elevation ($r^2 = 0.61$) due to the influence of elevation on temperature (equation (11)). The annual range of PET , $PET_{\max} - PET_{\min}$, is 6.5 mm d⁻¹, and $\sim 90\%$ of the station values fall within the range of 5.5–7.5 mm d⁻¹. The average lag of peak PET relative to peak solar forcing, L_{PET} , is 11 days and varies between 0 and 30 days across all stations. The average lag of PET minima relative to the minimum in solar forcing is also 11 days, and exhibits less variability from station to station. As discussed above, the timing of the wet season varies greatly across the southwest (Table 2). Therefore the lag between the middle of the wet season and peak ET, LAG (Figure 3), varies greatly between stations because L_{PET} is so consistent.

Table 4. Various Model Simulations Completed and the Range of Climate Parameters Specified in Each

Simulation Name	Precipitation			PET		LAG Between Peak P and PET
	\overline{P} , cm yr ⁻¹	τ_d and α	Rainfall Seasonality, f_w	\overline{PET} , cm yr ⁻¹	$PET_{\max} - PET_{\min}$, mm d ⁻¹	
Storm Size						
1.A: Typical	10–100	middle, Figure 4a	none	50–200	None	none
1.B: Maximum	10–100	top, Figure 4a	none	50–200	None	none
1.C: Minimum	10–100	bottom, Figure 4a	none	50–200	None	none
Season						
2.A: Rainfall only	10–100	equation (10)	0.15–0.5	150	0	none
2.B: PET only	10–100	equation (10)	0.5	150	6.4 mm d ⁻¹	none
2.C: LAG	10–100	equation (10)	0.32	150	6.4 mm d ⁻¹	0–360 days
Station	... ^a	... ^a	... ^a	... ^a	... ^a	... ^a

^aAccording to rainfall and temperature records at each station, 536 combinations.

3.3. Model Experiments

[33] For each simulation we take four steps to combine the climate parameterization and the flow model (bottom four panels in Figure 2). First, we select the values for each of the six climate parameters: \bar{P} , τ_d , f_w , \overline{PET} , $PET_{\max} - PET_{\min}$, and LAG . Second, we construct a time series of P and PET using these parameters. The rainfall record is 300 years long and is generated using random numbers selected from an exponential distribution [e.g., *Guswa et al.*, 2002]. The random numbers are scaled differently in the wet and dry seasons, as described in section 3.1. In contrast, the PET record does not include a stochastic component. The PET record is 1 year long, representing the average annual cycle. It is repeated 300 times to go along with the rainfall record. Third, the time series of P and PET are used as inputs to the flow model. Separate simulations are completed for loamy sand and loam soil, to assess how soils with different hydraulic properties modify the climatic controls on recharge. Fourth, the flux from the bottom of the domain is analyzed to assess if recharge occurred, as defined in equation (5).

[34] The simulations fall into three categories based on how the climate parameters are specified (Table 4 and top three boxes in Figure 2). In the first two types of simulations (storm size and season), we varied one or more of the six climate parameters over the range observed in the station data to quantify how they controlled recharge. In the third type of simulation (station), the full set of six climate parameters was set to the values observed for each station, yielding 536 realizations of climate.

[35] The storm size experiments were designed to assess how the distribution of storm size influences recharge. Three different groups of simulations were completed, using typical values of α and τ_d (equation (9) and solid line in Figure 4a) (1.A); maximum values for storm size (1.B); and minimum values for storm size (1.C). To constrain the end-member simulations, we fit envelopes to the $\tau_d - \bar{P}$ relationship. The upper line in Figure 4a shows how τ_d varies with \bar{P} where storms are large but occur infrequently. This relationship is used in the maximum storm size simulations. The bottom dashed line depicts the $\tau_d - \bar{P}$ relationship in locations where storms are small and frequent, and is used in the minimum storm size simulations. In all three cases, we varied \bar{P} and \overline{PET} over a broad range in different simulations. We did not include seasonality of P or PET , so these experiments are similar to other applications of the Poisson rainfall model to soil moisture dynamics [*Laio et al.*, 2001; *Guswa et al.*, 2002].

[36] The season simulations were designed to assess how seasonal fluctuations of P and PET influence recharge, over a broad range of \bar{P}/\overline{PET} . Typical values of α and τ_d were used (equation (9)) and were varied between the wet and dry season according to equation (10). The first set of simulations only included seasonality of precipitation (2.A, rainfall only), from no seasonality ($f_w = 0.5$) to high seasonality where 50% of the rainfall occurs in less than a 2-month period ($f_w = 0.15$). The second set only included seasonal fluctuations of PET (2.B, PET only). The third set included seasonality of both P and PET , with the lag between peak P and peak PET , LAG , varied from 0 to 360 days (2.C, LAG). PET seasonality, $PET_{\max} - PET_{\min}$, was set to 6.4 mm d^{-1} in all of the PET -only and LAG

simulations because variability of this parameter is limited (Table 3).

[37] In the station experiments, we used the six climate parameters calculated from each of the COOP station records to generate the rainfall and PET input time series. Therefore we generated 536 meteorological records, each representing the climate at one of the stations analyzed. The goal is not to predict at what locations recharge occurs, as this would require specifying z_r , soil texture, and other parameters for each site individually. The motivation for these experiments was to identify the most important controls on recharge, including possible interactions between seasonality and storm size distribution. By completing simulations using the full set of climate parameters derived from all the stations, we sampled over the complete distribution of combinations of seasonality, storm size, and other parameters.

4. Results

4.1. Storm Size Distribution

[38] Figure 6 shows that the percentage of precipitation that is partitioned to recharge (% R) varies as a function of \bar{P} in the storm size simulations, as expected. First, there is no recharge below a threshold \bar{P} value. This threshold depends on the combination of soil texture, \overline{PET} , and storm size used. Second, above the threshold, the amount of recharge increases with higher \bar{P} values. Vertical profiles of h for simulations with and without recharge are shown in Figure 7 for loamy sand. Results are similar for loam. For the case with recharge, wetting fronts propagate to the bottom of the domain; the maximum value of h at any point during the simulation is effectively zero at all depths. Throughout the root zone, mean h is much higher than h_{wilt} (-500 m or -5 MPa), but the minimum values show that $h \leq h_{wilt}$ at some time after initialization, so the soil does occasionally dry out. Below z_r , the soil remains wet throughout the simulation. For the case without recharge, the deepest wetting fronts only slightly exceed z_r and therefore do not reach the bottom of the domain yielding recharge. Above z_r , mean $h \approx h_{wilt}$, showing that the soil is typically very dry. As water movement below z_r is negligible, the mean, maximum, and minimum values all equal the initial h values (h_{wilt}) below the root zone.

[39] Quantifying how various aspects of climate control whether or not diffuse recharge occurs is the primary goal of this study. Therefore we identified the \bar{P}/\overline{PET} values that correspond to % R of 0.01% of \bar{P} , which is the recharge threshold described by equation (5). The storm size simulations yielded three main results (Figure 8). First, soil texture exerts a very strong control on the recharge threshold. For loamy sand, the lowest \bar{P}/\overline{PET} values at which recharge occurs vary from 0.4 to 0.8, depending on the storm size distribution and \overline{PET} . For loam, the lowest threshold value is >0.8 . A similar contrast exists for the \bar{P}/\overline{PET} value at which recharge exceeds 1% of \bar{P} . Second, the \bar{P}/\overline{PET} values at which % R equals the threshold and 1% decrease slightly as \overline{PET} increases for loamy sand. At higher PET values, storm depths are larger at the same values of \bar{P}/\overline{PET} , so the soil gets wetter and the potential for rapid gravity driven flow increases. For loam, the equivalent variations are smaller. Compared with the other factors

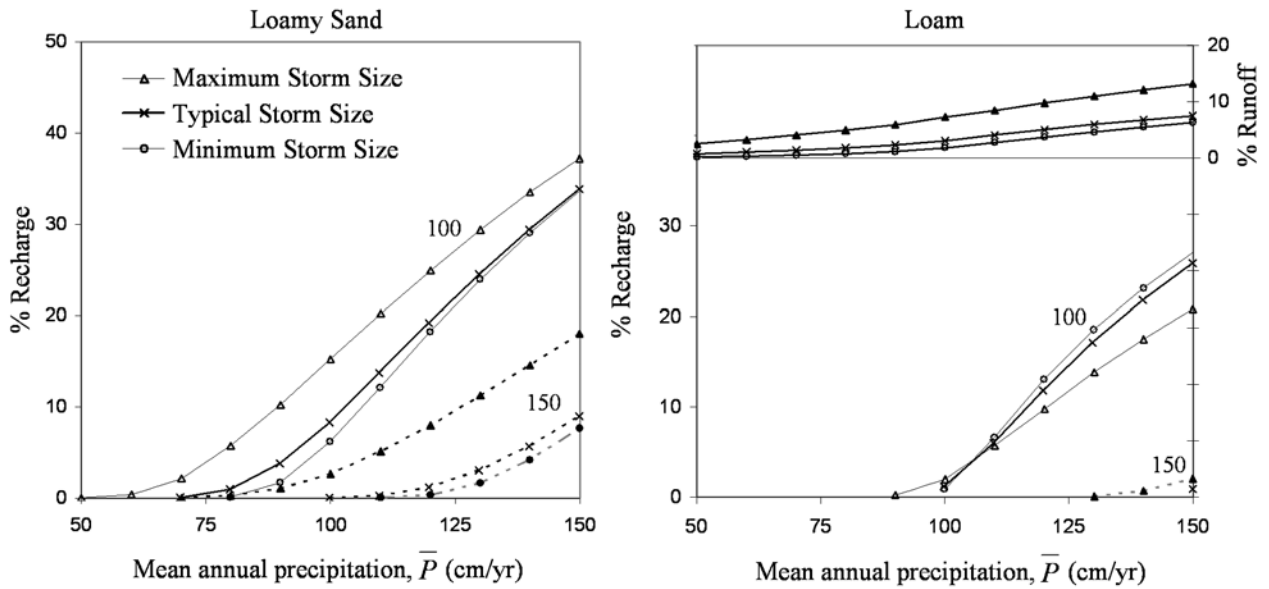


Figure 6. Variations in the percentage of rainfall that is partitioned to recharge, $\%R$, in the storm size experiments, for loamy sand and loam soil. The different storm size distributions are typical climate (crosses), maximum storm size (triangles), minimum storm size (circles). The value of \overline{PET} used is indicated by the type of the lines (solid = 100 cm yr^{-1} ; dashed = 150 cm yr^{-1}) and labeled on the graph. For loam, the top curves and right axis show how the percent of rainfall partitioned to runoff varies with \overline{P} , for $\overline{PET} = 100 \text{ cm yr}^{-1}$ only. Runoff is effectively zero for the loamy sand simulations.

examined, \overline{PET} has a negligible effect on $\%R$ at a given value of $\overline{P}/\overline{PET}$: roughly 0.05 over the range of \overline{PET} possible in semiarid environments. Therefore, when presented in terms of $\overline{P}/\overline{PET}$, our results are not sensitive to the actual \overline{PET} values used (equation (11)) but to the other factors such as seasonality and storm size distribution.

[40] Third, storm size distribution exerts a dramatic control on the recharge threshold for loamy sand: Recharge occurs at $\overline{P}/\overline{PET}$ values as low as 0.4 for a climate with large, infrequent storms (maximum storm size), compared with 0.8 for a climate with small, frequent storms (minimum storm size). This corresponds to recharge occurring at \overline{P}

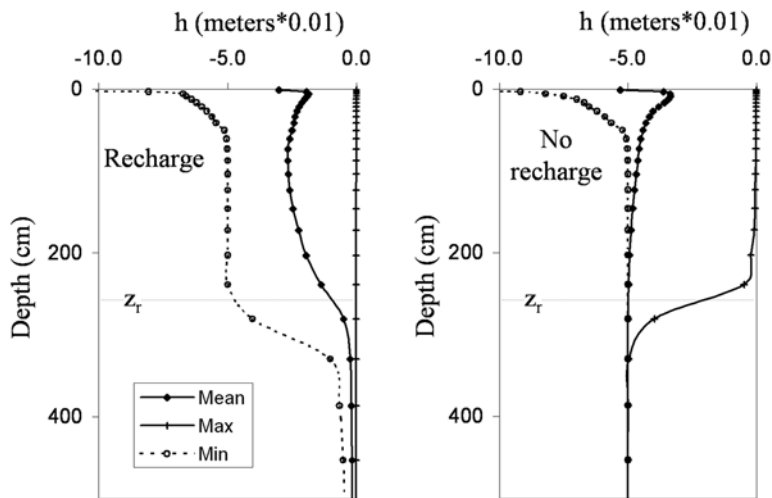


Figure 7. Vertical profiles of hydraulic head (h) for two loamy sand simulations, (left) one with recharge and (right) one without recharge. Units are meters \times 0.01, equivalent to soil water potential in MPa. Mean value is the average h at each depth between years 30 and 300 of the simulation. Minimum and maximum values show the extremes at each depth during the same interval. Therefore all three lines do not show h distribution at an instant in time. Only data from the top half of the simulated profiles are shown, and only half of the points in this portion of the profile are plotted for clarity. The horizontal dashed line is the maximum root depth, z_r . The wilting point, h_{wilt} , is -500 m (or -5.0 MPa).

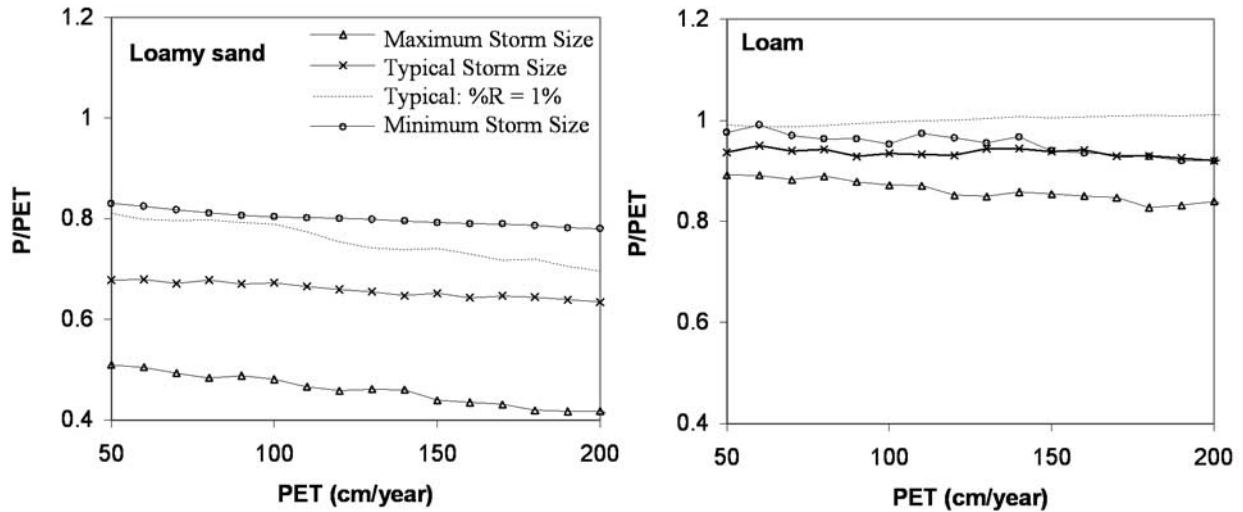


Figure 8. $\overline{P/PET}$ values at which the rainfall partitioned to recharge ($\%R$) is equal to 0.01% of \overline{P} , as a function of \overline{PET} . The 0.01% recharge threshold is the specified lower limit where the liquid-only flow model is applicable (equation (5)). Results are shown for climate with the typical, maximum, and minimum storm size distributions, for both loamy sand and loam soils. For the typical climate, the P/PET values at which $\%R = 1\%$ is also shown (dashed line). The climate parameters selected for each simulation (Table 4) did not yield $\%R$ of 0.01% and 1% exactly. Therefore we linearly interpolated to estimate the corresponding values of $\overline{P/PET}$, which is why the lines are not completely smooth.

of 60 versus 120 cm yr⁻¹, for $\overline{PET} = 150$ cm yr⁻¹. The results for the typical storm size climate are intermediate between the end-members. In contrast, for loam, the threshold and 1% R $\overline{P/PET}$ values are similar for the typical and minimum storm size climates, and lower by only ~ 0.1 for the maximum storm size climate.

[41] Storm size distribution influences the recharge threshold because it controls the frequency and duration of times when $P - PET$ exceeds zero and by how much. For the case of continuous rainfall (very low τ_d and α) in a climate where $\overline{P/PET} < 1$, the soil water content (θ) will never increase because $P - PET$ is never greater than zero, so recharge is not possible. Alternatively, for a climate

with large, infrequent storms, $P - PET$ is often greater than zero and θ can increase yielding recharge, as long as runoff is not substantial. The potential for recharge increases as the interval during which $P - PET$ exceeds zero increases: P may be several times higher than PET on the daily timescale, but individual storms will not add enough water to the soil to yield flow below the root zone.

[42] The percent of time when $P - PET > 0$ depends on storm size distribution: The frequency is higher for the maximum storm size climate than for the typical climate, which is higher than for the minimum storm size climate (Figure 9). In addition, the total water that accumulates

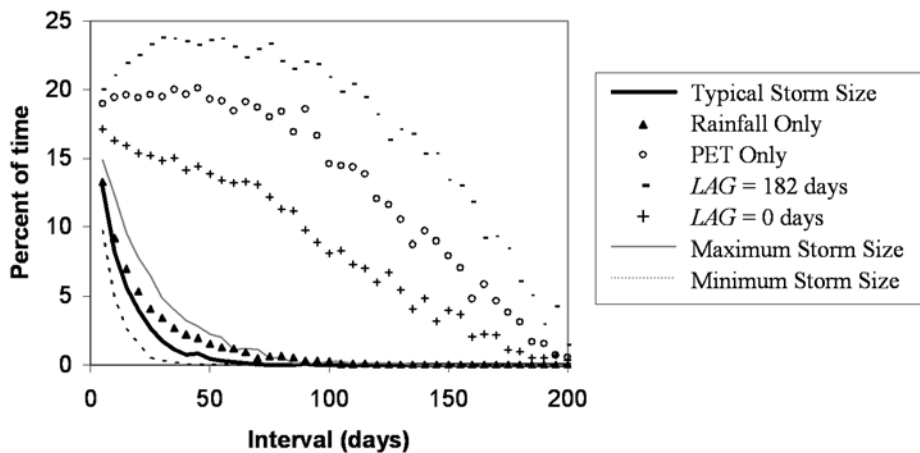


Figure 9. The percentage of time $P - PET > 0$ for each of the different climates simulated (see legend), plotted against different averaging intervals. The averaging intervals vary from 5 to 200 days, with a spacing of 5 days.

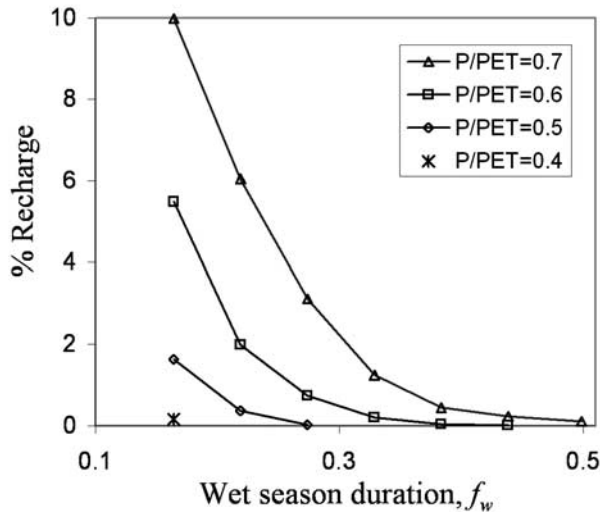


Figure 10. Percent of rainfall that is partitioned to recharge as a function of wet season duration, f_w , for loamy sand. \overline{PET} is 150 cm yr^{-1} in all cases, and the lines are for different values of $\overline{P}/\overline{PET}$.

during intervals when $P - PET > 0$ is greatest for the maximum storm size climate and least for the minimum storm size climate (not shown). Even with these differences, recharge through the loam soil is relatively insensitive to storm size distribution. This is partly due to the partitioning of rainfall to runoff, which amounts to 10% of rainfall for the maximum storm size climate and only 3% for the minimum storm size climate around the recharge threshold (Figure 6, right). In contrast, $<1\%$ of rainfall goes to runoff for loamy sand in all three climates around the recharge threshold.

[43] For both soils, once the recharge threshold is exceeded, much or all of the additional rainfall is partitioned to recharge (Figure 6). Runoff is negligible for the loamy sand, so all precipitation in excess of ET passes through the soil column and becomes recharge. A substantial fraction of rainfall becomes runoff for the loam (Figure 6, right), so $\%R$ does not increase as rapidly above the recharge threshold. The combination of a lower recharge threshold and less runoff results in more recharge through the loamy sand than through the loam, for any combination of \overline{P} , \overline{PET} , and storm size distribution (Figure 6).

[44] The influence of storm size distribution on the increase in $\%R$ above the recharge threshold is different for loamy sand and loam. For loamy sand, the greatest contrasts in $\%R$ exist around the recharge threshold: The most recharge occurs in the maximum storm size climate and the least in the minimum storm size climate. With increasing \overline{P} , $\%R$ from the different storm size simulations converges. For loam, differences in $\%R$ are small around the recharge threshold. However, as \overline{P} increases, the differences in $\%R$ between the three storm size distributions continuously grow. In addition, at higher values of \overline{P} , $\%R$ is greater for the minimum storm size climate than for the typical climate, and the value for the typical climate is greater than for the maximum storm size climate. This is opposite from the storm size contrasts for loamy sand and

is the result of more runoff for larger storms in the loam simulations.

4.2. Seasonality

4.2.1. Duration of Wet Season

[45] The first set of the three season experiments (2.A rainfall only, Table 4) was designed to assess the effects of wet season duration (f_w). We focus our discussion on the loamy sand simulations because there was no recharge in the loam simulations for reasonable values of \overline{PET} . A greater contrast in wet and dry season rainfall rates, equivalent to a shorter wet season or lower f_w , increases the fraction of rainfall that is partitioned to recharge (Figure 10). The $\overline{P}/\overline{PET}$ value of the recharge threshold decreases as seasonality increases (lower f_w). For loamy sand, recharge only occurs for cases when $\overline{P}/\overline{PET}$ is > 0.7 in the absence of a wet season (Figures 8 and 10). When the average ($f_w = 0.32$) and most intense ($f_w = 0.15$) wet seasons are used, the recharge threshold shifts to $\overline{P}/\overline{PET}$ of 0.5 and < 0.4 , respectively. Therefore the difference in recharge threshold across the range of f_w observed is equivalent to a shift of \overline{P} of more than 40 cm yr^{-1} , for $\overline{PET} = 150 \text{ cm yr}^{-1}$. This is similar to the difference of threshold $\overline{P}/\overline{PET}$ values for the minimum and maximum storm size distributions. Above the recharge threshold, $\%R$ increases as f_w decreases. In the next section we show that rainfall seasonality does not always enhance recharge as shown in Figure 10: Rainfall seasonality can decrease recharge via interactions with seasonal fluctuations of PET . The mechanism by which rainfall seasonality affects recharge is discussed below.

4.2.2. Seasonal Variation of Precipitation and PET

[46] We now compare the effects of seasonality of P and PET on recharge, using both the PET-only and lag simu-

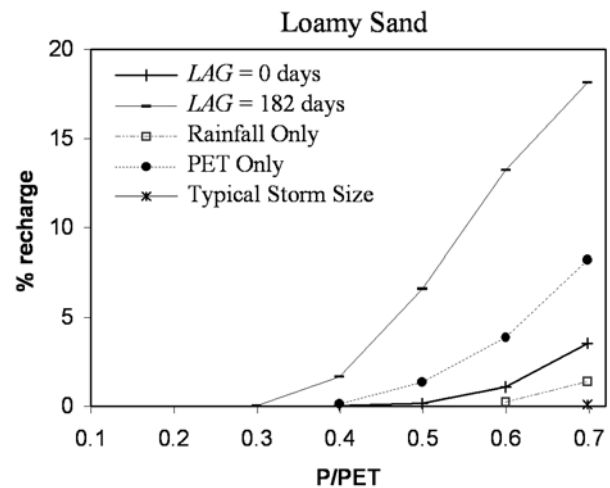


Figure 11. Percent of rainfall partitioned to recharge for different climates as a function of $\overline{P}/\overline{PET}$, for loamy sand. The “LAG = 0 days” line represents the case when the middle of the wet season occurs during the PET maximum, and the “LAG = 182 days” line is for the case when the middle of the wet season occurs during the PET minimum. The “annual values” line is for the case with no seasons (typical storm size in Table 4). \overline{PET} is 150 cm yr^{-1} in all cases. Results for loam are similar, except all lines are shifted to $\overline{P}/\overline{PET}$ values that are higher by 0.3.

Table 5. Notation and Calculations Used to Isolate the Component of Recharge Due to Different Factors^a

Notation	Simulation Includes Seasonal Variations of
f_{12}	P and PET
f_2	only P
$-f_1$	only PET
f_0	None

Calculations	Component of Recharge Due to
$\hat{f}_{12} = f_{12} - (f_1 + f_2) + f_0$	Interactions between P and PET seasonality
$\hat{f}_2 = f_2 - f_0$	P seasonality alone
$\hat{f}_1 = f_1 - f_0$	PET seasonality alone
$\hat{f}_0 = f_0$	factors other than seasonality

^aAfter Stein and Alpert [1993].

lations (2.B and 2.C, Table 4). In these experiments we use typical values of f_w , \overline{PET} , and $PET_{\max} - PET_{\min}$. \overline{P} is varied, yielding results for a range of $\overline{P}/\overline{PET}$ values. For loam we vary \overline{P} over a broader range than that found in semiarid environments (up to 165 cm yr⁻¹) so that the recharge threshold is exceeded in some experiments.

[47] The effects of seasonality are similar for loamy sand and loam soils (Figure 11), although the recharge threshold and equivalent values of %R for loam occur at $\overline{P}/\overline{PET}$ values that are higher by 0.3. First, including the typical annual cycle of PET greatly enhances recharge (PET only), lowering $\overline{P}/\overline{PET}$ of the recharge threshold by 0.3, compared with a climate with no seasonality. This effect is much greater than that which results from including the typical seasonality of rainfall alone (rainfall only). Second, when the P and PET maxima are out of phase ($LAG = 182$ days), including both seasonal cycles enhances recharge compared with the case where only PET varies. This case represents a climate where the wet season occurs during the middle of the winter. When the cycles are in phase ($LAG = 0$ days), including both seasonal cycles yields less recharge. This represents a climate where the wet season occurs during the summer.

[48] In summary, there is a consistent order of how recharge varies between the different simulations. From most to least recharge, the order is (1) out of phase P and PET seasonal cycles ($LAG = 182$ days); (2) PET cycle only; (3) in phase P and PET cycles ($LAG = 0$ days); (4) P cycle only; and (5) no seasonality of P or PET . Clearly, consideration of only annual values provides limited information regarding the existence and amount of recharge, given the importance of seasonality on flow through the root zone (Figure 11) and the predominance of seasonality in semiarid environments (Tables 2 and 3). For loamy sand, the simulated recharge threshold occurs at a $\overline{P}/\overline{PET}$ value <0.3 when typical values for seasonality are included, compared with 0.7 for the case with no seasons.

[49] To quantify the portion of recharge resulting from each seasonal forcing alone and from their interactions, we use the numerical factor analysis described by Stein and Alpert [1993] summarized in Table 5. The results are similar for both soils, although shifted to higher $\overline{P}/\overline{PET}$ values for loam. Near the recharge threshold, nearly 100% of the recharge is due to interactions between seasonality of P and PET when the seasonal cycles are out of phase (Figure 12). As $\overline{P}/\overline{PET}$ increases, the component of

recharge due to seasonal variations in PET alone increases, and equals that caused by $P - PET$ interactions at the highest $\overline{P}/\overline{PET}$ values simulated. Rainfall seasonality alone only contributes to recharge at $\overline{P}/\overline{PET}$ values greater than 0.6 for loamy sand, and even then the contribution is minor. Little or no recharge occurs without the seasonal cycles of P and PET .

[50] Figure 13 shows how recharge varies as a function of the lag (LAG) between the seasonal maxima of P and PET . The most recharge occurs when peak PET lags the middle of the wet season by half a year ($LAG = 182$ days). For the lowest $\overline{P}/\overline{PET}$ value used (0.3), recharge only occurs when LAG is between 100 and 300 days. For all values of \overline{P} , the least recharge occurs when peak ET occurs during the middle of the wet season ($LAG = 0$ days). Variations between the maximum and minimum recharge values are sinusoidal and nearly symmetric.

[51] Seasonality of P and PET affect recharge in the same way as storm size distribution: When $P - PET > 0$, water accumulates in the root zone and can lead to recharge. \overline{P} may be much less than \overline{PET} . However, the intervals when $P - PET > 0$ are more common when seasonality is introduced. Compared with a climate without seasons, typical rainfall seasonality ($f_w = 0.32$) in the absence of PET variations (rainfall only) increases the occurrences of when $P - PET > 0$ only slightly (Figure 9). This makes sense given that the rainfall rate during the 4-month wet season is only ~60% higher than the annual average, so P is still less than PET averaged throughout the wet season. In contrast, including the annual cycle of PET (PET only) greatly increases the fraction of the year when $P - PET > 0$

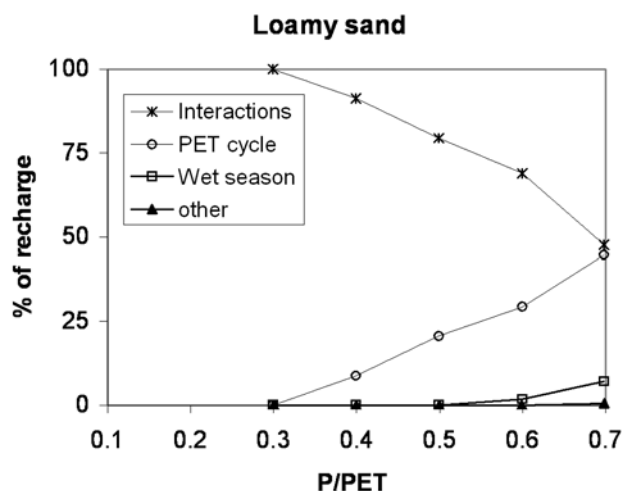


Figure 12. The percent of simulated recharge through loamy sand resulting from the following four factors as a function of $\overline{P}/\overline{PET}$, determined via factor separation analysis (Table 5): (1) interactions between P and PET seasonality ($LAG = 182$ days); (2) PET seasonality; (3) P seasonality; and (4) other effects. The results shown in this figure are only for simulations with a half-year lag between peak PET and the middle of the wet season ($LAG = 182$ days); the wet season occurs during the winter. Results for loam are very similar, except all lines are shifted to $\overline{P}/\overline{PET}$ values that are higher by 0.3.

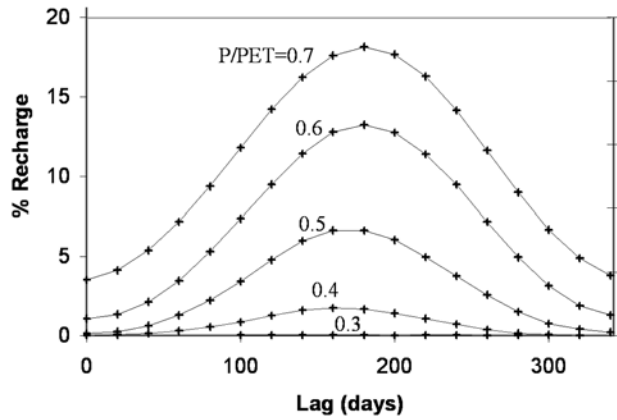


Figure 13. Variations in % R with different values of LAG between peak PET and the middle of the wet season, for a range of different $\overline{P/PET}$ values. Results for loam are similar.

and the excess P that accumulates during those intervals. When P and PET maxima are lagged by half a year ($LAG = 182$ days), the wet season enhances the effects of PET seasonality on the distribution of $P - PET$. The reverse occurs when the P and PET cycles are in phase ($LAG = 0$ days). The results from the recharge and $P - PET$ analyses are consistent: The ranking of different climates in terms of recharge (Figure 11) is the same as the ranking of climates in terms of how frequently $P - PET > 0$ for all time intervals examined.

4.3. Climate Parameters From Each Station Record

[52] In the station simulations, we used the climate parameters derived from each station record to assess how the observed combinations of storm size and seasonality influence recharge. Consistent with the other results, recharge through loam soil was limited, only exceeding the 0.01% \overline{P} threshold for 10 of the 536 parameter combinations. At these 10 stations, the $\overline{P/PET}$ are 10 of the 15 highest observed at all stations. In contrast, when the loamy sand was used, diffuse recharge occurred for 116 of the 536 parameter combinations, or just over 20% (Figure 14, top portion). At these stations, the average $\overline{P/PET}$ was 0.4 and the minimum was 0.21, compared with the data set average of 0.25. Slightly more than 50% of all 536 stations have $\overline{P/PET}$ values that exceed 0.21, so recharge only occurred for stations that fall in the top half of the $\overline{P/PET}$ distribution. These stations were at higher than average elevation and were preferentially located in northern portions of Utah, Nevada, New Mexico, eastern California, and along the Mogollon Rim in Arizona. We focus the remainder of our discussion on the results from the loamy sand simulations.

[53] For loamy sand, % R is generally higher for higher values of $\overline{P/PET}$ (Figure 14, bottom portion). When $\overline{P/PET} > 0.4$, recharge occurs for all parameter combinations. In the $\overline{P/PET}$ range of 0.2–0.4, recharge occurs for some parameter combinations ($n = 82$) but not for others ($n = 164$). Recharge does not occur when $\overline{P/PET} < 0.2$. Recharge occurs at many more stations than would be predicted for a climate without seasons but with the same $\overline{P/PET}$: % R from

the station simulations is higher than for either the typical or maximum storm size simulations. In addition, the recharge calculated using the station climate parameters is always higher than for a climate with seasonal maxima of P and PET that are in phase ($LAG = 0$ days). Many of the parameter combinations that yield recharge are clustered around the line for a climate where seasonal fluctuations of P and PET are out of phase ($LAG = 182$ days).

[54] We now identify why there is recharge for only one third (84 of 266) of the parameter combinations with $\overline{P/PET}$ values between 0.2 and 0.4. Any combination of the factors shown to influence recharge in sections 4.1 and 4.2 could produce these results (Table 6). For stations with $\overline{P/PET}$ between 0.2 and 0.4, the intensity of rainfall seasonality is lower (higher f_w) for the 84 stations that have recharge than for those that do not (Table 6). However, the magnitude of the difference is small and the sensitivity to this parameter is relatively limited. Both wet (α_{wet}) and dry season (α_{dry}) storm sizes are slightly lower for the stations with recharge, which should also limit recharge. Stations with recharge tend to have slightly higher values of $PET_{max} - PET_{min}$, which should increase recharge slightly. Most important, the stations with recharge have substantially longer lags between P and PET maxima than the stations without recharge, 117 and 54 days, respectively. Given that longer lags greatly increase the presence and amount of recharge (Figure 13), this is clearly an important factor differentiating the two sets of parameter combinations. The lag values are even

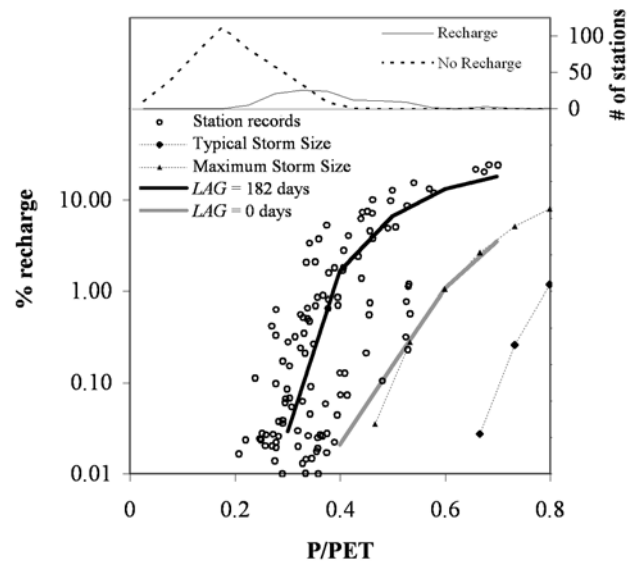


Figure 14. Number of stations with and without simulated recharge for loamy sand, binned in $\overline{P/PET}$ increments of 0.05, are shown in top portion of the panel. Bottom portion shows % R as a function of $\overline{P/PET}$ for COOP stations in the western United States. Recharge is above the specified threshold ($q_b > 0.0001 \times \overline{P}$ or % $R = 0.01$) for 116 of the 536 stations with long P and T records. The remaining 420 cases (no recharge) are not plotted. Results from some of the storm size and season simulations are plotted for reference.

Table 6. Summary Statistics for Station Parameter Combinations With $\overline{P/PET}$ Between 0.2 and 0.4, Split Into Stations With and Without Recharge

	Recharge	No Recharge	p-Value ^a
<i>n</i>	80	182	
$PET_{\max} - PET_{\min}$, mm d ⁻¹	6.3 ± 0.5	6.1 ± 0.5	0.006
<i>LAG</i>	117 ± 58	54 ± 44	<0.001
<i>f_w</i>	0.34 ± 0.08	0.30 ± 0.07	<0.001
α_{wets} , cm	0.71 ± 0.27	0.79 ± 0.27	0.008
α_{dry} , cm	0.59 ± 0.15	0.61 ± 0.16	0.15

^aShows results from a one-tailed t-test.

more extreme (146 days) for the 25 stations with recharge that have $\overline{P/PET}$ values between 0.2 and 0.3.

5. Discussion and Conclusions

[55] Our results show that comparisons of mean annual precipitation and potential evapotranspiration alone will not yield accurate predictions of where diffuse recharge will occur. Over the range of climate and soils texture examined here, $\overline{P/PET}$ values at the recharge threshold varied from 0.2 to 0.7. Even lower values are possible for soils that are coarser than the loamy sand used here. There is substantial variability in storm size distribution across the southwestern United States. For coarse soils, a climate with relatively large but infrequent storms should have a lower $\overline{P/PET}$ recharge threshold than a climate with smaller, more frequent storms, changing the $\overline{P/PET}$ at the recharge threshold by 0.3 between extreme end-member climates. The effects are much smaller for fine-textured soils.

[56] Seasonality has a larger influence on recharge than storm size distribution, and the effects are similar for both coarse and fine soils. Across the southwestern United States, there is a wide range in the magnitude of rainfall seasonality but comparatively little variability in seasonality of *PET*. However, diffuse recharge is relatively insensitive to rainfall seasonality. In addition, the magnitude of rainfall seasonality can lower or raise the $\overline{P/PET}$ value of the recharge threshold, depending on whether the wet season occurs in the winter or summer, respectively. By itself, the annual cycle of *PET* enhances recharge and lowers $\overline{P/PET}$ of the recharge threshold more than any other factor investigated. However, all stations have relatively similar *PET* annual cycles. Therefore the magnitude of seasonal *PET* fluctuations is probably not an important source of differences in recharge between locations. Instead, the relative timing of *P* and *PET* maxima is the primary factor that controls the presence or absence of recharge: The most recharge will occur when the rainy season occurs during the winter months when *PET* values are lowest.

[57] Overall, the results presented here are consistent with the conclusions drawn from data-based studies of recharge through desert vadose zones. First, our results show there should be no diffuse recharge in arid climates ($\overline{P/PET} = 0.1$), regardless of soil texture or the presence of wintertime precipitation. This is consistent with data collected at low elevation areas in the Mojave desert of California and Nevada [Tyler *et al.*, 1996; Izbicki *et al.*, 2000], although exceptions may exist when soils are extremely coarse

[Barnes *et al.*, 1994]. Second, for intermediate values of $\overline{P/PET}$ (0.2–0.4), our modeling shows there should be no diffuse recharge on fine soils, but diffuse recharge may occur on coarser soils depending upon the climate at the site. This result is consistent with observations that show there is no recharge at sites with $\overline{P/PET}$ of 0.2–0.4 that are located on fine-textured soils or in locations where summer rainfall dominates, for example, in the High Plains and Chihuahuan sites described by Scanlon *et al.* [2003]. It is also consistent with lysimeter data from Hanford, Washington [Gee *et al.*, 1994], which showed deep percolation beneath vegetation in a winter wet climate with $\overline{P/PET} = 0.1$. Additional vadose zone profile data should be collected in locations where $\overline{P/PET} < 0.4$ and rainfall that is concentrated during the winter. Third, our modeling results are consistent with the idea that recharge occurred at many southwestern sites during the last glacial period. Many sites in this region have $\overline{P/PET}$ values close to the simulated recharge threshold. Therefore only small changes in \overline{P} or \overline{PET} are necessary for the threshold to be crossed, particularly if the climate shifts include changes in seasonality that enhance recharge.

[58] Although this research was focused on understanding how climate influences recharge, not all aspects of climate were represented. The effects of the accumulation and melt of snow on recharge were not evaluated. We expect that incorporating snow would increase the importance of wet seasons that occur during winter, given that springtime melt would deliver most of the moisture in a single pulse. The effects of relative humidity and wind speed on *PET* calculations are not represented in the Hargreaves model, as they are in the more detailed Penman-Monteith approach. Both of these issues should be addressed in future research. The model of climate developed here allowed us to evaluate how six key parameters influenced recharge. However, the rainfall records generated do not include all of the complexity of actual time series. For example, intervals with anomalously dry or wet conditions may not be accurately simulated by the Poisson rainfall model. To ensure that the synthetic rainfall records were reasonable, we ran the model using actual rainfall data, repeating station records as needed to yield 300 years of rainfall inputs. Ten stations with recharge and 10 stations without recharge in the station simulations were randomly selected for this analysis. Other than the rainfall input, all other aspects of these model runs were identical to the station simulations. In all 20 cases, the presence or absence of recharge was the same for the synthetic and actual rainfall records. For the cases with recharge, the amount of recharge simulated using actual rainfall data was very similar to that simulated using the synthetic records: A regression between the paired values had an r^2 of 0.89 and a slope of 0.93. In general, the use of actual records yielded slightly more recharge.

[59] The model simulations described here are idealized with regards to many factors. Vertical variations in soil texture were not specified, including the presence and characteristics of caliche. Horizontal variability in soil texture was also not considered, which could focus flow in some situations and lead to recharge at even lower $\overline{P/PET}$ values [Kearns and Hendrickx, 1998]. Soil texture affects vertical root distributions [Schenk and Jackson, 2002], but

we did not vary root profiles between the different soils used in the simulations. We represented vegetation in our model by specifying typical parameter values for desert plants. However, values for these parameters vary with plant type and soil texture [Schenk and Jackson, 2002]. In addition, more complex models for soil water extraction by roots exist [Sperry, 2000; Guswa et al., 2002]. A more detailed focus on vegetation would be necessary in order to use the model presented here to test the hypothesis that the shift to desert vegetation ~10 kyr stopped diffuse recharge at many locations [Phillips, 1994].

[60] **Acknowledgments.** This research was supported by SAHRA (Sustainability of Semi-Arid Hydrology and Riparian areas) under the STC Program of the National Science Foundation, Agreement 9876800. Comments from three anonymous reviewers, Fred Phillips, and John Wilson were very helpful.

References

- Allen, R. G., L. S. Pereira, D. Raes, and M. Smith (1998), Crop evapotranspiration: Guidelines for computing crop requirements, *Irrig. Drain. Pap.*, 56, U.N. Food and Agric. Organ., Rome.
- Allison, G. B., W. J. Stone, and M. W. Hughes (1985), Recharge in karst and dune elements of a semi-arid landscape as indicated by natural isotopes and chloride, *J. Hydrol.*, 76, 1–25.
- Allison, G. B., P. G. Cook, S. R. Barnett, G. R. Walker, I. D. Jolly, and M. W. Hughes (1990), Land clearance and river salinisation in the western Murray Basin, Australia, *J. Hydrol.*, 119, 1–20.
- Andraski, B. J. (1997), Soil-water movement under natural-site and waste-site conditions: A multiple-year field study in the Mojave Desert, Nevada, *Water Resour. Res.*, 33, 1901–1916.
- Barnes, C. J., G. Jacobson, and G. D. Smith (1994), The distribution recharge mechanism in the Australian arid zone, *Soil Sci. Soc. Am. J.*, 58, 31–40.
- Beverly, C. R., R. J. Nathan, K. W. J. Malafant, and D. P. Fordham (1999), Development of a simplified unsaturated module for providing recharge estimates to saturated groundwater models, *Hydrol. Processes*, 13, 653–675.
- Canadell, J., R. B. Jackson, J. R. Ehleringer, H. A. Mooney, O. E. Sala, and E. D. Schulze (1996), Maximum rooting depth of vegetation types at the global scale, *Oecologia*, 108, 583–595.
- Droogers, P., and G. Allen (2002), Estimating reference evapotranspiration under inaccurate data conditions, *Irrig. Drain. Syst.*, 16, 33–45.
- Eagleson, P. S. (1978), Climate, soil, and vegetation: Introduction to water balance dynamics, *Water Resour. Res.*, 14, 705–712.
- Edmunds, W. M., W. G. Darling, and D. G. Kinniburgh (1988), Solute profile techniques for recharge estimation in semi-arid and arid terrain, in *Estimation of Natural Groundwater Recharge*, edited by I. Simmers, pp. 139–157, Springer, New York.
- Fayer, M. J., G. W. Gee, M. L. Rockhold, M. D. Freshley, and T. B. Walters (1996), Estimating recharge rates for a groundwater model using a GIS, *J. Environ. Qual.*, 25, 510–518.
- Feddes, R. A., et al. (2001), Modeling root water uptake in hydrological and climate models, *Bull. Am. Meteorol. Soc.*, 82, 2797–2809.
- Gee, G. W., et al. (1994), Variations in water balance and recharge potential at three western desert sites, *Soil Sci. Soc. Am. J.*, 58, 63–72.
- Grismer, M. E., S. Bachman, and T. Powers (2000), A comparison of groundwater recharge estimation methods in a semi-arid, coastal avocado and citrus orchard (Ventura County, California), *Hydrol. Processes*, 14, 2527–2543.
- Guswa, A. J., M. A. Celia, and I. Rodriguez-Iturbe (2002), Models of soil moisture dynamics in ecohydrology: A comparative study, *Water Resour. Res.*, 38, 1166, doi:10.1029/2001WR000826.
- Hargreaves, G. H., and Z. A. Samani (1982), Estimating potential evapotranspiration, *J. Irrig. Drain. Div. Am. Soc. Civ. Eng.*, 108(3), 225–230.
- Hawk, K. L., and P. S. Eagleson (1992), Climatology of station storm rainfall in the continental United States: Parameters of the Bartlett-Lewis and Poisson rectangular, *Rep. 336*, Ralph M. Parsons Lab. for Water Resour. and Hydrodyn., Mass. Inst. of Technol., Cambridge, Mass.
- Hendrickx, J. M. H., and G. R. Walker (1997), Recharge of phreatic aquifers in (semi-) arid areas, in *Recharge From Precipitation*, edited by I. Simmers, chap. 2, pp. 19–111, A. A. Balkema, Brookfield, Vt.
- Hevesi, J. A., A. L. Flint, and L. E. Flint (2002), Preliminary estimates of spatially distributed net infiltration and recharge for the Death Valley region, Nevada-California, *U.S. Geol. Surv. Water Resour. Invest. Rep.*, 02-4010, 36 pp.
- Houston, J. (2002), Groundwater recharge through an alluvial fan in the Atacama Desert, northern Chile: Mechanisms, magnitudes and causes, *Hydrol. Processes*, 16, 3019–3035.
- Huang, K., B. P. Mohanty, and M. T. van Genuchten (1996), A new convergence criterion for the modified Picard iteration method to solve the variably saturated flow equation, *J. Hydrol.*, 178, 69–91.
- Izbicki, J. A., J. Radyk, and R. L. Michel (2000), Water movement through a thick unsaturated zone underlying an intermittent stream in the western Mojave Desert, southern CA, USA, *J. Hydrol.*, 238, 194–217.
- Johnston, C. D. (1987), Preferred water flow and localized recharge in a variable regolith, *J. Hydrol.*, 94, 129–142.
- Keams, A., and J. M. H. Hendrickx (1998), Temporal variability of diffuse groundwater recharge in New Mexico, *Rep. 309*, N. M. Water Resour. Res. Inst., N. M. State Univ., Las Cruces.
- Lai, C. T., and G. Katul (2000), The dynamic role of root-water uptake, *J. Hydrometeorol.*, 530, 427–439.
- Laio, F., et al. (2001), Plants in water-controlled ecosystems: Active role in hydrologic processes and response to water stress, *Adv. Water Resour.*, 24, 707–723.
- Leaney, F. W., and A. L. Herczeg (1995), Regional recharge to a karst aquifer estimated from chemical and isotopic composition of diffuse and localized recharge, south Australia, *J. Hydrol.*, 164, 363–387.
- Mahfouf, J., C. Ciret, A. Ducharme, P. Irannejad, J. Noilhan, Y. Shao, P. Thornton, Y. Xue, and Z. Yang (1996), Analysis of transpiration results from the RICE and PILPS workshop, *Global Planet. Change*, 13, 73–88.
- Mann, J. F. (1976), Wastewaters in the vadose zone of arid regions: Hydrologic interactions, *Groundwater*, 14, 367–373.
- Nativ, R. (1991), Radioactive waste isolation in arid zones, *J. Arid Environ.*, 20, 129–140.
- Phillips, F. M. (1994), Environmental tracers for water movement in desert soils of the American southwest, *Soil Sci. Soc. Am. J.*, 58, 15–24.
- Pockman, W. T., and J. S. Sperry (2000), Vulnerability to cavitation and the distribution of Sonoran desert vegetation, *Am. J. Bot.*, 87, 1287–1299.
- Rockhold, M. L., M. J. Fayer, C. T. Kincaid, and G. W. Gee (1995), Estimation of natural groundwater recharge for the performance assessment of a low-level waste disposal facility at the Hanford Site, *Rep. PNL-10508*, Pac. Northwest Natl. Lab., Richland, Wash.
- Rodriguez-Iturbe, I., A. Porporato, L. Ridolfi, V. Isham, and D. R. Cox (1999), Probabilistic modeling of water balance at a point: The role of climate, soil and vegetation, *Proc. R. Soc. London A*, 455, 3789–3805.
- Ross, B. (1984), A conceptual model of deep unsaturated zones with negligible recharge, *Water Resour. Res.*, 20, 1627–1629.
- Scanlon, B. R. (1992), Moisture and solute flux along preferred pathways characterized by fissured sediments in desert soils, *J. Contam. Hydrol.*, 10, 19–46.
- Scanlon, B. R., R. P. Langford, and R. S. Goldsmith (1999), Relationship between geomorphic settings and unsaturated flow in an arid setting, *Water Resour. Res.*, 35, 983–1000.
- Scanlon, B. R., K. Keese, R. C. Reedy, J. Simunek, and B. J. Andraski (2003), Variations in flow and transport in thick desert vadose zones in response to paleoclimatic forcing (0–90 kyr): Field measurements, modeling, and uncertainties, *Water Resour. Res.*, 39, 1179, doi:10.1029/2002WR001604.
- Schaap, M. G., F. J. Leij, and M. T. van Genuchten (1998), Neural network analysis for hierarchical prediction of soil hydraulic properties, *Soil Sci. Soc. Am. J.*, 62, 847–855.
- Schenk, H. J., and R. B. Jackson (2002), The global biogeography of roots, *Ecol. Monogr.*, 72, 311–328.
- Scott, R. L., et al. (2000), Modeling multiyear observations of soil moisture recharge in the semiarid American southwest, *Water Resour. Res.*, 36, 2233–2247.
- Shuttleworth, W. J. (1993), Evaporation, in *Handbook of Hydrology*, edited by D. Maidment, pp. 4.1–4.53, McGraw-Hill, New York.
- Simunek, J., M. Sejna, and M. T. van Genuchten (1998), The HYDRUS-1D software package for simulating the one-dimensional movement of water, heat, and multiple solutes in variably saturated media, Version 2.0, *Rep. IGWMC-TPS-70*, Int. Ground Water Model. Software, Int. Ground Water Model. Cent., Golden, Colo.
- Sorman, A. U., M. J. Abdulrazzak, and H. J. Morel-Seytoux (1997), Groundwater recharge estimation from ephemeral streams: Case study: Wadi Tabalah, Saudi Arabia, *Hydrol. Processes*, 11, 1607–1619.

- Sperry, J. S. (2000), Hydraulic constraints on plant gas exchange, *Agric. For. Meteorol.*, 104, 13–23.
- Stein, U., and P. Alpert (1993), Factor separation in numerical simulations, *J. Atmos. Sci.*, 50, 2107–2115.
- Stephens, D. B. (1994), A perspective on diffuse natural recharge mechanisms in areas of low precipitation, *Soil Sci. Soc. Am. J.*, 58, 40–48.
- Stephens, D. B., and R. Knowlton Jr. (1986), Soil water movement and recharge through sand at a semiarid site in New Mexico, *Water Resour. Res.*, 22, 881–889.
- Tyler, S. W., J. B. Chapman, S. Conrad, D. Hammermiester, D. Blout, J. Miller, M. Sully, and J. Ginanni (1996), Soil water flux in the southern Great Basin, United States: Temporal and spatial variations over the last 120,000 years, *Water Resour. Res.*, 32(6), 1481–1499.
- van Dam, J. C., and R. A. Feddes (2000), Numerical simulation of infiltration, evaporation and shallow groundwater levels with the Richards equation, *J. Hydrol.*, 233, 72–85.
- van Dam, J. C., J. G. Huygen, J. G. Wesseling, R. A. Feddes, P. Kabat, P. E. V. van Walsum, P. Groenendijk, and C. A. Van Diepen (1997), SWAP version 2.0: Theory: Simulation of water flow, solute transport and plant growth in the soil-water-air-plant environment, *Tech. Doc. 45*, DLO Winand Staring Cent., Wageningen, Netherlands.
- van Genuchten, M. (1980), A closed-form equation for predicting the hydraulic conductivity of unsaturated soils, *Soil Sci. Soc. Am. J.*, 44, 892–898.
- Walvoord, M., M. A. Plummer, F. M. Phillips, and A. V. Wolfsberg (2002a), Deep arid system hydrodynamics: 1. Equilibrium states and response times in thick desert vadose zones, *Water Resour. Res.*, 38, 1308, doi:10.1029/2001WR000824.
- Walvoord, M., F. M. Phillips, S. W. Tyler, and P. C. Hartsough (2002b), Deep arid system hydrodynamics: Application to paleohydrologic reconstruction using vadose-zone profiles from the northern Mojave Desert, *Water Resour. Res.*, 38, 1291, doi:10.1029/2001WR000825.
- Wood, W. W., and W. E. Sanford (1995), Chemical and isotopic methods for quantifying ground-water recharge in a regional, semiarid environment, *Ground Water*, 33, 458–468.

E. E. Small, Department of Geological Sciences, University of Colorado, Campus Box 399, 2200 Colorado Avenue, Boulder, CO 80309-0399, USA. (eric.small@colorado.edu)

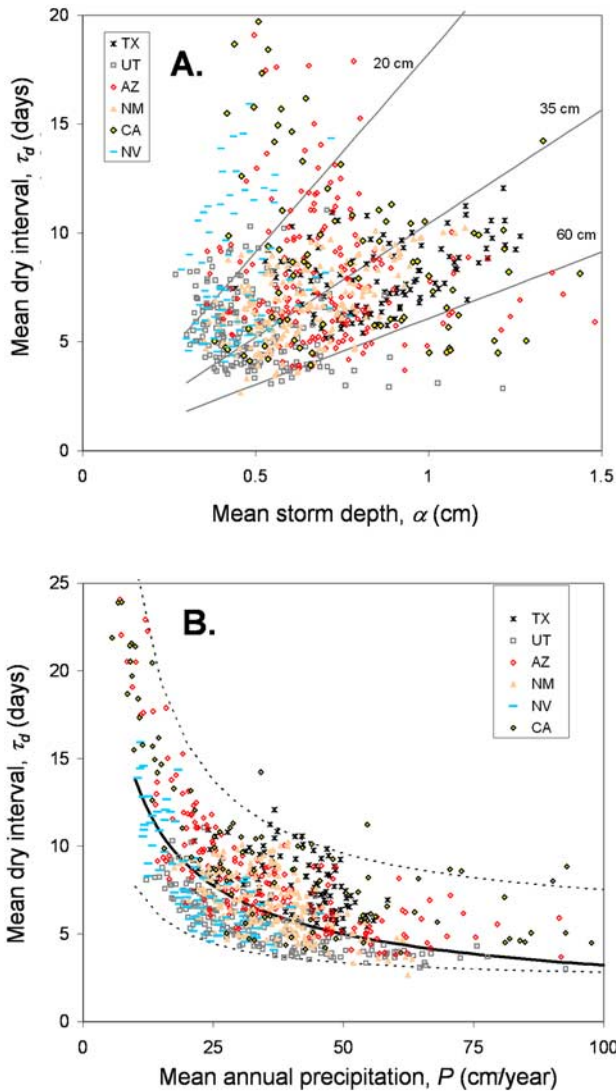


Figure 4. (a) Mean dry interval (τ_d) versus mean storm depth (α) for southwestern U.S. stations. The various symbols represent the different states. Lines of equal \bar{P} are drawn and labeled. (b) Relationship between τ_d and \bar{P} . The solid line is the best fit power law curve to all data points ($r^2 = 0.51$), used in the “typical storm size” simulations (Table 4). Dashed lines are envelopes using the same equation form, with parameters selected so that the lines encompass all but the extreme outliers. The top dashed curve represents the $\tau_d - \bar{P}$ relationship where dry intervals are long and storms are large, used in the “maximum storm size” simulations. The bottom line represents the $\tau_d - \bar{P}$ relationship where storms are frequent but small, used in the “minimum storm size” simulations.

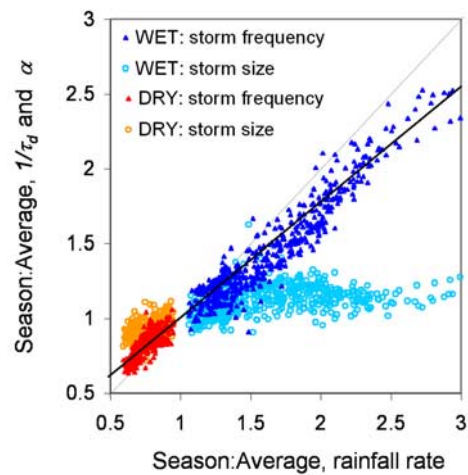


Figure 5. Scatterplot of the ratios of season-to-average $1/\tau_d$ (triangles) and α (circles) versus the ratio of season-to-average rainfall rates for all COOP stations. The ratios for both the wet (light and dark blue points) and dry (orange and red symbols) seasons are shown. The thin line is the 1:1 line, and the thick line is the best fit linear regression to the normalized wet and dry season $1/\tau_d$ values (equation (10)).